Chemical Engineering Science 161 (2017) 127–137

Contents lists available at ScienceDirect

Chemical Engineering Science

journal homepage: www.elsevier.com/locate/ces

Kinetic modelling of the hematin catalysed decolourization of Orange II solutions

Cecilia Cabrera [a,1], Andrés Cornaglia [a,1], Agostina Córdoba [b,*], Ivana Magario [c], María Lujan Ferreira [d]

[a] Facultad de Ciencias Exactas, Físicas y Naturales – Universidad Nacional de Córdoba, Córdoba, Argentina
[b] Centro de Investigación y Tecnología Química (CITeQ), Universidad Tecnológica Nacional – CONICET, Córdoba, Argentina
[c] Investigación y Desarrollo en Tecnología Química (IDTQ), Grupo Vinculado PLAPIQUI-CONICET, Facultad de Ciencias Exactas, Físicas y Naturales – Universidad Nacional de Córdoba, Córdoba, Argentina
[d] Planta Piloto de Ingeniería Química (PLAPIQUI)-CONICET, Universidad Nacional del Sur, Bahía Blanca, Argentina

ARTICLE INFO

Article history:
Received 1 August 2016
Received in revised form 26 November 2016
Accepted 30 November 2016
Available online 8 December 2016

Keywords:
Kinetic study
Hematin
Orange II
H_2O_2 dismutation
Dynamic modelling

ABSTRACT

A mathematical description of the kinetics of the hematin catalysed decolourization reaction of Orange II alkaline solutions was constructed and validated under the assumption that hematin mimics the action of peroxidases. The clean oxidant H_2O_2 was applied, however, hematin dismutated it, as catalases do, under reaction conditions. Thus, special attention was cared to the understanding of this ineffective side-reaction by the proposal of straightforward pathways concerning the catalatic or the pseudo-catalatic cycles. Model validations were implemented by a parametrization procedure of relevant rate constants under dynamic simulation fitting to selected experimental time-courses data. The peroxidatic coupled to pseudo-catalatic mechanism gave predictions closer to experimental findings in a wide range of conditions. The initial rate method for data processing was successfully applied for providing reliable initial rate constant guesses but also for the detection of unexpected rate depletion at high dye concentrations. This was considered in the model as unproductive dye coordination to hematin native state prior to H_2O_2 activation. The pseudo-catalatic pathway involves the production of superoxide and its coordination to hematin native state to afford inactive but regenerable ferrous porphyrin. Model underestimations of experimental data were interpreted as cooperative oxidation of Orange II molecules by superoxide whereas model deviations at high dye concentration (>400 mg/l) was assigned to further hematin catalysed oxidation of Orange II degraded products.

1. Introduction

Textile wastewaters have different composition depending on the kind of fabrics produced at the particular industry. Nevertheless, all of them are characterized by high values of pH, chemical oxygen demand (COD) and biochemical oxygen demand (BOD) (Centro Panamericano de Ingeniería Sanitaria y Ciencias del Ambiente, 1994, 1997). The effluents generated during the dyeing step reach 65% of the total wastewater (Lachheb et al., 2002). Different technologies focusing on synthetic dyes degradation have been developed based on model studies. Orange II (OII, C.I. 15510) is one of the most used azoic dyes (Hunger, 2003) and it has been extensively studied as model compound (Cardona et al., 2009; Gong et al., 2010; Hai et al., 2009; Lodha and Chaudhari, 2007).

Chemicals methods named as Advanced Oxidation Processes (AOPs) include the generation of hydroxyl radical ($OH^{\cdot}$), able to degrade the organic matter. The most studied AOPs methods are Fenton and Fenton-like. Iron salts catalyse hydroxyl radical formation (Babuponnusami and Muthukumar, 2014; Chen and Zhu, 2010; Liang et al., 2010; MacKay and Pignatello, 2001). However, those systems required acidic pH to achieve high yields. Biological treatments use bacteria or fungi to degrade organic contaminants. Mono and di-oxygenases of these organisms can catalyse oxygen incorporation at double bonds in aromatic compounds (Saratale et al., 2011). Synthetic dyes with azo or sulfonic groups are recalcitrant because of their resistance to oxygenases (Saratale et al., 2011). In order to improve the efficiencies of biological treatments, enzymatic methods have been successfully developed. Excellent results of peroxidase-mediated OII decolourization have been published (López et al., 2004a,b; Yousefi and Kariminia, 2010). The removal of phenolic pollutants from aqueous solutions catalysed by Horseradish Peroxidase (HRP) has been extensively studied

* Corresponding author.
E-mail address: agostinacordoba@gmail.com (A. Córdoba).
[1] Both authors contributed equally to this work.

http://dx.doi.org/10.1016/j.ces.2016.11.049
0009-2509/

(Bhunia et al., 2001; Hamid and Khalilur, 2009; Nicell et al., 1995; Ulson de Souza et al., 2007; Wagner and Nicell, 2002). However, spite of high performance in phenolics oxidation using peroxidases, several drawbacks arose including: (1) enzyme's high cost, (2) H_2O_2-mediated inactivation and (3) organic radicals-mediated inactivation, among others.

Biomimetic systems based on synthetic or natural, porphyrinic or nonporphyrinic metal complexes have been studied as replacement of enzymes in synthetic dyes degradation (Ambrosio et al., 2004; Hodges et al., 1997; Pirillo et al., 2010a,b; Zucca et al., 2008). Our research group published promising results about the use of hematin as a HRP biomimetic (Córdoba et al., 2012a,b, 2015). Hematin is a natural IX-ferry-protoporphyrin analogous to the active site of HRP and catalases (Sheldon, 1994). At least 92% conversion of OII (75 mg L^{-1}) after 1 h -hematin/H_2O_2 treatment- was obtained corresponding to azo bond cleavage followed by degradation into aromatic and aliphatic carboxylic acids (Córdoba et al., 2012a). Indeed, response surface analysis was implemented to determine the effects of operational conditions (temperature, pH, oxidant and catalyst concentration). Temperature (in the range 30–50 °C) was a statistically insignificant factor on conversion as well as on catalytic efficiency (defined as mmol of converted OII per gram of catalyst, per mmol of oxidant) according the experimental design results analysis. This was not an expected result and it was interpreted as typical for reaction mechanisms involving radicals.

HRP oxidation mechanism (i.e. peroxidatic mechanism) and its inactivation routes have been studied by different authors (Dunford, 1999, 2002; Hernández-Ruiz et al., 2001; Hiner et al., 2001; Loew et al., 1997; Nicell and Wright, 1997; Reihmann and Ritter, 2006; Rich and Iwaki, 2007; Veitch, 2004; Vlasits et al., 2010; Vojinovic et al., 2004). HRP-catalysed hydrogen abstraction from reducing substrates has been confirmed (Buchanan and Nicell, 1997; Dunford, 1999; Reihmann and Ritter, 2006). Different metalloporphyrin oxidation mechanisms have been deeply discussed (Bruice et al., 1988; Hodges et al., 1997; Rebelo et al., 2005; Stephenson and Bell, 2007a; Traylor and Xu, 1987). Nam, Bell and coworkers proposed a Fenton-based mechanism with Fe (II) intermediates species and homolytic cleavage of the peroxidic bond (O—O) of H_2O_2 (Bell et al., 1991; Nam et al., 2000, 2001; Stephenson and Bell, 2005). However, heterolytic O—O cleavage with formation of an oxoperferryl π-cation radical (as the analogous to HRP species E_1) is widely accepted (Nam et al., 2000; Stephenson and Bell, 2005; Traylor and Xu, 1990).

In a previous work by our group a peroxidatic model for phenol oxidation based on the HRP reaction mechanism was proposed for hematin. UV–visible analysis and kinetic modeling results were in line with formation of Compound I and II (E_1 and E_2) (Córdoba et al., 2015). On the other hand, O_2 production was observed in phenol/H_2O_2 systems only with hematin, in line with the existence of an effective "catalatic-pathway", i.e. catalytic H_2O_2 dismutation ($2\ H_2O_2 \rightarrow 2\ H_2O + O_2$). Hernández-Ruiz, Hiner and coworkers modelled the HRP catalatic-like activity as a single coordination reaction between E_1 and H_2O_2 to E_0, analogous to catalases (Hernández-Ruiz et al., 2001; Hiner et al., 2001). Besides, Vlasits and coworkers reviewed the mechanism of catalase activity of heme peroxidases and postulated a pseudo-catalatic mechanism involving hydroperoxyl radical formation (HOO·) (Vlasits et al., 2010). During the study of phenol polymerization, Akkara et al. suggested an hematin oxidation mechanism with E_1 and E_2 formation and a catalatic pathway (Akkara et al., 2000). Based on this scenario, the peroxidatic mechanism was proposed for decolourization of Orange II solution catalysed by hematin but coupled to two other possible mechanisms for peroxide dismutation named as *catalatic* and *pseudo-catalatic*. Scheme 1 shows the mechanisms analyzed in this work.

In order to determine experimental values of rate constants, linearization strategies of concentration-time curves as well as the application of kinetic methods have been successfully applied (Buchanan and Nicell, 1997; Gómez et al., 2006; Hammami et al., 2008; Nicell, 1994). Tizaoui et al. published a kinetic modelling study of azo dyes decolourization based on the ozone oxidation mechanism of Orange 16 (Tizaoui and Grima, 2011). In addition, there are reports of kinetic modelling of photocatalytic degradation of dyes by Ultraviolet (UV)/TiO_2 (Daneshvar et al., 2004; Sleiman et al., 2007), as well as photo-oxidative treatments (UV/H_2O_2) (Daneshvar et al., 2008; Modirshahla and Behnajady, 2006). However, to the best of our knowledge, there is no published kinetic analysis of hematin catalytic action toward phenolics or peroxide dismutation. Earlier manuscripts focused on the involvement of heme proteins on *in vivo* peroxidation and hydroperoxide formation (Rafiquzzaman et al., 1995; Van Der Zee et al., 1996).

The objective of this study is to obtain a validated decolourization model based on mechanistic aspects related to Orange II degradation by soluble hematin. Meanwhile, the model could be applied for the design of a decolourization stage for textile effluents treatment process. Reaction mechanisms were proposed and mathematically described for hematin-catalysed Orange II decolourization. Kinetic experiments at selected conditions were carried out for its validation. Two methodologies were pursued: (1) the inspection of initial rates and preliminar estimation of rate constant values; and; (2) the utilization of the entire Orange II concentration profile during reaction for a parametrization procedure of rate constants. The first approach applies the assumption of the pseudo steady-state condition for the catalytic intermediates of

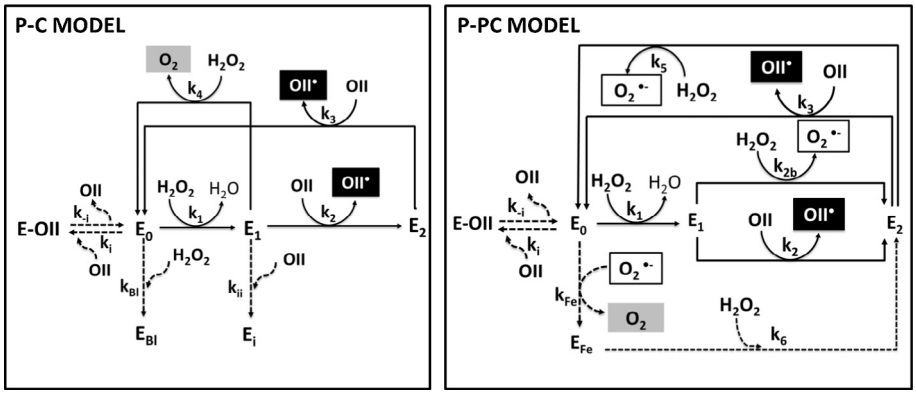

Scheme 1. Peroxidatic and Catalatic Mechanisms. P-C MODEL: Peroxidatic coupled to catalatic pathway; P-PC MODEL: Peroxidatic coupled to pseudo-catalatic pathway. Dash lines denote added routes to original pathways in order to interpret experimental data.

hematin in order to find algebraic expressions based on measurable variables, whereas the second approach considers non-steady state conditions for all species involved. The determination of activation energy was excluded of this kinetic study, especially when temperature was demonstrated of insignificant importance in the range considered (Córdoba et al., 2012a). Temperature was always set constant for all trials at the minimum value of the studied range (30 °C).

2. Modelling

The kinetic models were based on mass balances of reactants, products and catalyst intermediates. Decolourization P-C model denotes the peroxidatic pathway coupled to catalatic whereas the P-PC model indicates the peroxidatic pathway coupled to pseudo-catalatic (see Scheme 1). The P-C model involved 7 equations and 8 rate constants:

$$\frac{d[E_0]}{dt} = -k_1[E_0][H_2O_2] + k_4[E_1][H_2O_2] + k_3[E_2][OII] - k_{Bl}[E_0][H_2O_2] - k_i[E_0][OII] + k_{-i}[E-OII] \quad (1)$$

$$\frac{d[E_1]}{dt} = k_1[E_0][H_2O_2] - k_4[E_1][H_2O_2] - k_2[E_1][OII] - k_{ii}[E_1][OII] \quad (2)$$

$$\frac{d[E_2]}{dt} = k_2[E_1][OII] - k_3[E_2][OII] \quad (3)$$

$$\frac{d[E_{Bl}]}{dt} = k_{Bl}[E_0][H_2O_2] \quad (4)$$

$$\frac{d[E-OII]}{dt} = k_i[E_0][OII] - k_{-i}[E-OII] + k_{ii}[E_1][OII] \quad (5)$$

$$\frac{d[H_2O_2]}{dt} = -k_1[E_0][H_2O_2] - k_4[E_1][H_2O_2] - k_{Bl}[E_0][H_2O_2] \quad (6)$$

$$\frac{d[OII]}{dt} = -k_2[E_1][OII] - k_3[E_2][OII] - k_i[E_0][OII] + k_{-i}[E-OII] - k_{ii}[E_1][OII] \quad (7)$$

Meanwhile, the P-PC model involved 8 equations and 10 rate constants:

$$\frac{d[E_0]}{dt} = -k_1[E_0][H_2O_2] + k_5[E_2][H_2O_2] + k_3[E_2][OII] - k_{Fe}[E_0][O_2^{\cdot-}] - k_i[E_0][OII] + k_{-i}[E-OII] \quad (8)$$

$$\frac{d[E_1]}{dt} = k_1[E_0][H_2O_2] - k_{2b}[E_1][H_2O_2] - k_2[E_1][OII] - k_{ii}[E_1][OII] \quad (9)$$

$$\frac{d[E_2]}{dt} = k_{2b}[E_1][H_2O_2] - k_5[E_2][H_2O_2] + k_2[E_1][OII] - k_3[E_2][OII] + k_6[E_{Fe}][H_2O_2] \quad (10)$$

$$\frac{d[E_{Fe}]}{dt} = k_{Fe}[E_0][O_2^{\cdot-}] - k_6[E_{Fe}][H_2O_2] \quad (11)$$

$$\frac{d[E-OII]}{dt} = k_i[E_0][OII] - k_{-i}[E-OII] + k_{ii}[E_1][OII] \quad (12)$$

$$\frac{d[H_2O_2]}{dt} = -k_1[E_0][H_2O_2] - k_{2b}[E_1][H_2O_2] - k_5[E_2][H_2O_2] - k_6[E_{Fe}][H_2O_2] \quad (13)$$

$$\frac{d[OII]}{dt} = -k_2[E_1][OII] - k_3[E_2][OII] - k_i[E_0][OII] + k_{-i}[E-OII] - k_{ii}[E_1][OII] \quad (14)$$

$$\frac{d[O_2^{\cdot-}]}{dt} = -k_{2b}[E_1][H_2O_2] + k_5[E_2][H_2O_2] - k_{Fe}[E_0][O_2^{\cdot-}] + k_{-i}[E-OII] - k_{ii}[E_1][OII] \quad (15)$$

For systems without OII both models also apply but the terms involving OII concentration cancel (Section 4.3). Note that mass balances for OII and E-OII are identical in both models and are eliminated for systems without OII.

Change of absorbance at selected wavelength was interpreted as OII consumption during reaction.

The assumptions in the models with OII present were:

- Upon OII coordination to E_1 or E_2 hematin species, a hydrogen atom is abstracted from the phenolic group of OII and a radical OII· is formed.
- This radical species undergoes further rapid reactions whose rates are much higher than the hydrogen abstraction step.
- OII reaction products do not appreciably contribute to the absorbance.
- OII reaction products do not interact with hematin, OII or H_2O_2 molecules.

2.1. Parametrization procedure

In order to estimate the rate constants of the proposed models software gPROMS 3.2 (General Process Modeling System, Process System Enterprise Ltd., London, UK) was used. The parameter estimation tool of gPROMS have been employed to solve the problem of estimation based on model information, initial values for each of the kinetic constants and boundary conditions for each differential equation. One advantage of gPROMS lies in the possibility of dynamic modeling i.e. uses experimental data from transients and steady states for parameterization. This function is based on the simultaneous evaluation of two kinds of parameters, kinetic constants of proposed model and the parameters of a user-selected variance model for experimental data (Process Systems Enterprise, 2004). This estimation process uses intrinsic solvers consisting of numerical algorithms whose function is to solve the problem by iterative numerical methods. MAXLKHD solver of gPROMS following the method of maximum likelihood was employed (Process Systems Enterprise, 2004). The standard DASOLV solver was used for the integration of the model equations. The parameter estimation tool applies a χ^2 (95%) statistical test to determine the goodness of fit.

Upon parameterization of both models, the initial concentrations of catalyst (E_0) and of H_2O_2 were set based on the experimental conditions, while the initial concentrations of catalytic intermediates and of peroxyl radicals were zero. The constant variance model ($\sigma^2 = \omega^2$) was selected in all cases.

The sensitivity of the rate constants was determined by evaluating global sensitivity analysis of the dynamic model, for which simulations were conducted with initial values of the constants and variations of ±20% thereof.

Initial guesses of rate constants to be parametrized were carefully set, when possible, by the initial rates method and otherwise assumed according to published values for HRP or synthetic phorpyrins. Thus, at t = 0 pseudo steady-state of hematin intermediates was assumed in order to find algebraic expressions relating initial rates and initial OII, hematin and H_2O_2 concentrations. The sum of the hematin intermediates was assumed to be equal to the total hematin added (E_n):

$E_n = E_0 + E_1$ (for derivation of equation 16)

$E_n = E_0 + E_1 + E_2$ (for derivation of equation 17 and 18)

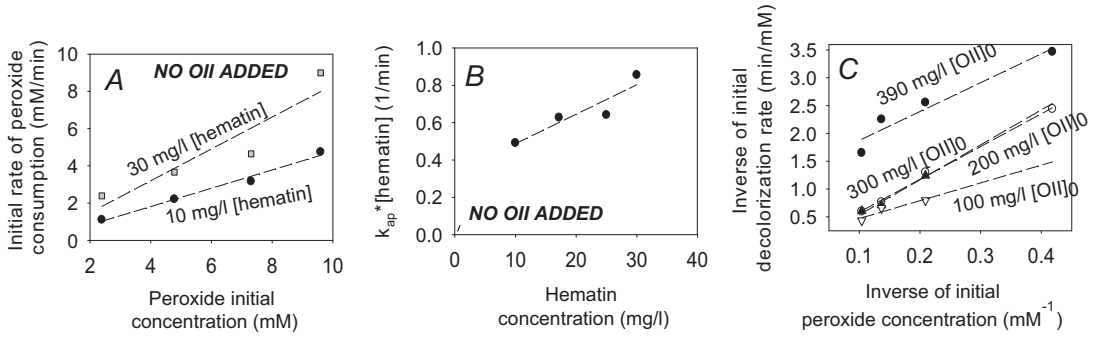

Fig. 1. Effect of hematin and peroxide concentrations on initial rates. (A and B) peroxide consumption without OII addition. (C) OII consumption. Hematin concentration was fixed at 10 mg/l for assays of (C).

Thus, mass balance of OII (Eq. (7)) was derived to Eq. (18) and mass balance of H_2O_2 (Eq. (6) or (13)) was derived in Eq. (16) or (17), respectively. Eqs. (16)–(18) were then fitted to experimental observations in order to find initial guesses of rate constants for the parametrization procedure. Eq. (18) was adjusted to experimental data through an expression involving the summation of the quadratic differences between experimental rates and the rate obtained by Eq. (18) at the corresponding initial concentrations.

3. Experimental

3.1. Materials

Hematin (molecular weight: 633.49) was provided by Sigma Co. (San Luis, USA) and was used without further purification. OII (C.I.:15510, molecular weight: 350.32) was supplied by Merck KGaA (Darmstadt, Germany). Hydrogen peroxide 30 vol.% was obtained from Laboratorios Apotarg SRL (Córdoba, Argentina). Buffer solutions were prepared with double-distilled water and carbonate/bicarbonate salts of analytical grade.

3.2. Kinetic assay

Reactions were carried in glass flasks using carbonate/bicarbonate 0.01 M buffer solution pH 10.6, with magnetic stirring at 30 °C and 50 ml reaction volume. Fifteen experiments without OII were carried on, varying hydrogen peroxide concentration between 2.4 mM to 9.6 mM and hematin concentration from 10 to 30 mg/l. 1 ml samples were withdrawn at different times interval during reaction and the H_2O_2 concentration was determined by iodometric titration. Meanwhile, twenty-nine dye degradation experiments were carried on. OII concentration was varied between 5 and 400 mg/l; hematin concentration was 3, 10 or 17.2 mg/l; and the hydrogen peroxide concentrations were 2.4, 4.7, 7.3 and 9.6 mM. Samples (0.1–1 ml) were withdrawn at different time intervals after hydrogen peroxide addition (t = 0 min) and diluted in H_2SO_4 1 M in order to stop the reaction. These samples were analyzed by UV–Vis spectroscopy at 484 nm (ε_{484} = 19.5 mM^{-1} cm^{-1}). A Perkin Elmer Lambda 35 spectrophotometer (Massachusetts, USA) was used for these measurements. Finally, H_2O_2 concentration after 40 min reaction was determined by iodometric titration for selected experiments.

4. Results and discussion

4.1. Initial rates of peroxide and OII consumption

A 0.1 M carbonate/bicarbonate buffer solution (pH 10.6) induced a decrease of 48% of $[H_2O_2]$ when initial value of $[H_2O_2]$ was 11.5 mM (in the absence of hematin). Therefore, the buffer concentration was fixed to 0.01 M, where no decrease of $[H_2O_2]$ was detected at similar experimental conditions. Fig. 1A shows variation of initial rates of peroxide consumption with increasing peroxide initial concentration and indicates first-order kinetics. The slopes of the curves in Fig. 1A increased with increasing hematin concentration also in a linear fashion thus indicating first order kinetic for hematin (see Fig. 1B). According to Scheme 1, without OII addition, only the catalatic (or pseudo-catalatic) loop is operative. The rate law at t = 0 under steady state assumption of hematin intermediates resulted in:

$$-r_{0,H2O2} = \underbrace{2k_4 \Big/ \left(\frac{k_4}{k_1}+1\right)}_{k_{ap}} \cdot [H_2O_2]_0[E_n] \quad \text{from C model} \tag{16}$$

$$-r_{0,H2O2} = \underbrace{3k_5 \Big/ \left(\frac{k_5}{k_1}+\frac{k_5}{k_{2b}}+1\right)}_{k_{ap}} \cdot [H_2O_2]_0[E_n] \quad \text{from PC model} \tag{17}$$

Note that it was assumed that k_{BI} and k_{Fe} are both much lower than k_1 ($E_{BI,t=0}$ = 0; $E_{Fe,t=0}$ = 0). Both pathways may apply to explain the trend of initial rates in Fig. 1A and B with an apparent rate constant (k_{ap}) of 10 ± 2 mM^{-1} min^{-1}.

Fig. 2 presents the variation of initial reaction rate of OII consumption with increasing OII initial concentration. Typical saturation curves were observed with maxima values varying with the applied peroxide concentration. Initial rates decreased abruptly after the maxima resembling some kind of hematin inhibition caused by OII. Several mechanisms can be proposed. Coordination of one or more OII molecules with some/all the hematin intermediary states is supposed to take place (Pirillo et al., 2010a). Because native hematin does not react with OII, we first assumed that it coordinates to one OII molecule and blocking its peroxide activation. Secondly, since H_2O_2 was dosed to an equilibrated OII/hematin, this coordination was considered reversible since otherwise no reaction would have taken place. Taking into account this inhibition step in the P-C model (Scheme 1), the initial rate of OII consumption equals to:

$$-r_{0,OII} = \frac{2[E_n]}{\frac{1}{[H_2O_2]_0}\left[\frac{1}{k_1}\left(1+K_I[OII]_0\right)\right] + \left(\frac{k_1k_2+k_3k_4}{k_1k_2k_3}\right)\frac{1}{[OII]_0} + \frac{k_1K_I}{k_1k_2}} \tag{18}$$

In Eq. (18) K_I denotes the equilibrium constant (k_i/k_{-i}) for the coordination step between E_0 and the OII. k_{ii} was assumed to be zero and the inequality $k_2 \gg k_3$ was taken as in the case of peroxidases (Dunford, 1999). Fig. 1C shows the tendency of initial rates of OII consumption with variation of peroxide initial concentrations in a reciprocal fashion. The linear fitting is in agreement to Eq. (18). Moreover, the increase of slopes observed with increasing OII concentration gives support to the idea of an inhibition step.

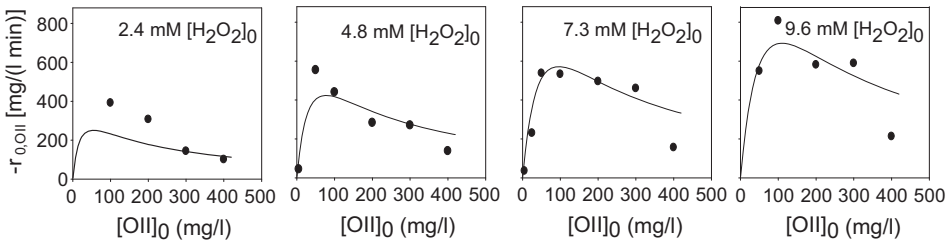

Fig. 2. Effect of initial OII concentrations on initial decolourization rates (points). Continues lines give the fitting by Eq. (18). Hematin concentration was fixed at 10 mg/l for all assays.

The factor $[OII] * K_I$ masks the k_1 estimation. Therefore, an average of all four slopes ($6.6 \pm 2.2\ mM^{-1}\ min^{-1}$) was taken as an initial guess for k_1 in the parametrization procedure of the C-model (Section 4.3). Meanwhile, from Eqs. (16) and (17) initial guesses of k_4 ($20.9\ mM^{-1}\ min^{-1}$) and k_{2b} ($13.8\ mM^{-1}\ min^{-1}$) could be obtained and taken as an initial guesses of parametrization of C-model and PC-model, respectively. Lines in Fig. 2 represent Eq. (18) after a fitting procedure to the experimental points. For this, k_1 value was fixed to the optimized value obtained after parametrization of the C-model (Section 4.3) whereas k_3 was fixed at 10% of k_2 value, as normally found in peroxidases (Dunford, 1999). Values of $2.37\ mM^{-1}$ and $7694\ mM^{-1}\ min^{-1}$ were found for K_I and k_2, respectively.

4.2. Kinetics of hematin-mediated H_2O_2 dismutation

Hydrogen peroxide dismutation presented a biphasic exponential profile with a high initial reaction rate followed by a much lower one. Clearly, some kind of deactivation using hematin was taking place during the reaction. Therefore, parametrization of the C-model of Scheme 1 was unable to predict these tendencies. In an early study, we have observed a peroxide-dependent bleaching of the Soret band of hematin at the same reaction conditions (Córdoba et al., 2012b). We first proposed an inactivation reaction upon interaction of H_2O_2 to E_0 with E_{BI} formation, in line with Cunningham et al. (2001) on metalloporphyrin (F_{20}TPPFeCl) during oxidation of alkenes. The initial guess value (k_{BI}) was 16 times lower than k_1. Preliminar estimations resulted in a statistically accurate model but optimized constants values were not statistically significant. Therefore, every rate constant was subjected to a sensitivity analysis. Only k_4 was ranked as irrelevant and was therefore fixed for the remaining parametrization task. The result is presented in Table 1. The model passed the "good fit" test and both constants (k_1 and k_{BI}) have been optimized. Fig. 3 shows the agreement between experimental and modelled H_2O_2 consumption profiles (continue lines). At H_2O_2 initial concentration lower than 5 mM model fit is acceptable. However, it was not able to simulate the $[H_2O_2]$ profiles at higher peroxide concentrations. The inclusion of an inactivation effect of hydrogen peroxide as the bleaching route from hematin E_1 or the consideration that the "bleached state" still presents some partial activity did not improve fitting of the model to experimental data (data not shown).

The catalatic loop does not admit formation of $OOH^{\cdot}$, $O_2^{\cdot-}$ or $OH^{\cdot}$. In a prior study, we observed oxygen evolution on HRP and hematin catalysed oxidations at neutral pH and suggested the involvement of inorganic radical species in hematin-mediated systems (Córdoba et al., 2015). To account for these the called *pseudo-catalatic* pathway (PC-model) was implemented (Scheme 1) (Paolo Zucca and Sanjust, 2014; Stephenson and Bell, 2007b; Vlasits et al., 2010). Indeed, the catalytic state E_1 is reduced upon two one-electron reductions affording state E_2 and finally the resting state E_0. Both steps generate hydroperoxyl radicals ($OOH^{\cdot}$), which under alkaline conditions dissociates to superoxide (pK 4.8) (Dunford, 2002):

$$OOH^{\cdot} \leftrightarrow O_2^{\cdot-} + H^+$$

The uncatalysed dismutation of superoxide to dioxygen is not favoured at high pHs (Dunford, 1999; Song and Zhang, 2008). On the other hand, Dunford (2002) clearly reviewed evidence in opposition to the uncatalysed Haber-Weiss reaction. Superoxide can however transfer one electron to Fe(III) – E_0-thereby resulting in Fe(II) -E_{Fe}- and dioxygen. This reaction is widely accepted for iron included in metal complexes (Oh-Kyu Lee, 2002), in porphines (Paolo Zucca and Sanjust, 2014) and even in heme peroxidases (Vlasits et al., 2010). In peroxidases a stable inactive intermediate called Compound III (E_3) is formed:

Table 1
Initial guesses and optimized rate constants values of catalatic and pseudo-catalatic H_2O_2 decomposition.

Catalatic model			Pseudo-catalatic model			
	Initial guess ($mM^{-1}\ min^{-1}$)	Optimized		Initial guess ($mM^{-1}\ min^{-1}$)	Optimized	Peroxidases***
k_1	6.6	$16.4_{\pm 1.5}$	k_1	16.4*	16.4*	$>10^5$
k_4*	20.9*	20.9*	k_{2b}	13.8	60.2**	10^{-3}
k_{BI}	0.4	$0.33_{\pm 0.03}$	k_5	6.0****	90.3**	10^{-2}
			k_{Fe}	0.3	$3.5_{\pm 0.7}$	–
			k_6	4200***	$0.026_{\pm 0.006}$	10^3
Initial guess of σ^2		0.1^2		0.1^2		
Optimized σ^2		$0.29^2_{\pm 0.03}$		0.5^{**2}		
Residuals		127.0		204.9		
χ^2 (95%)		150.9		209.0		

* Fixed value during parameter estimation.
** Non-optimized parameter value.
*** Hiner et al. (2001), Vlasits et al. (2010).
**** Cunningham et al. (2001).

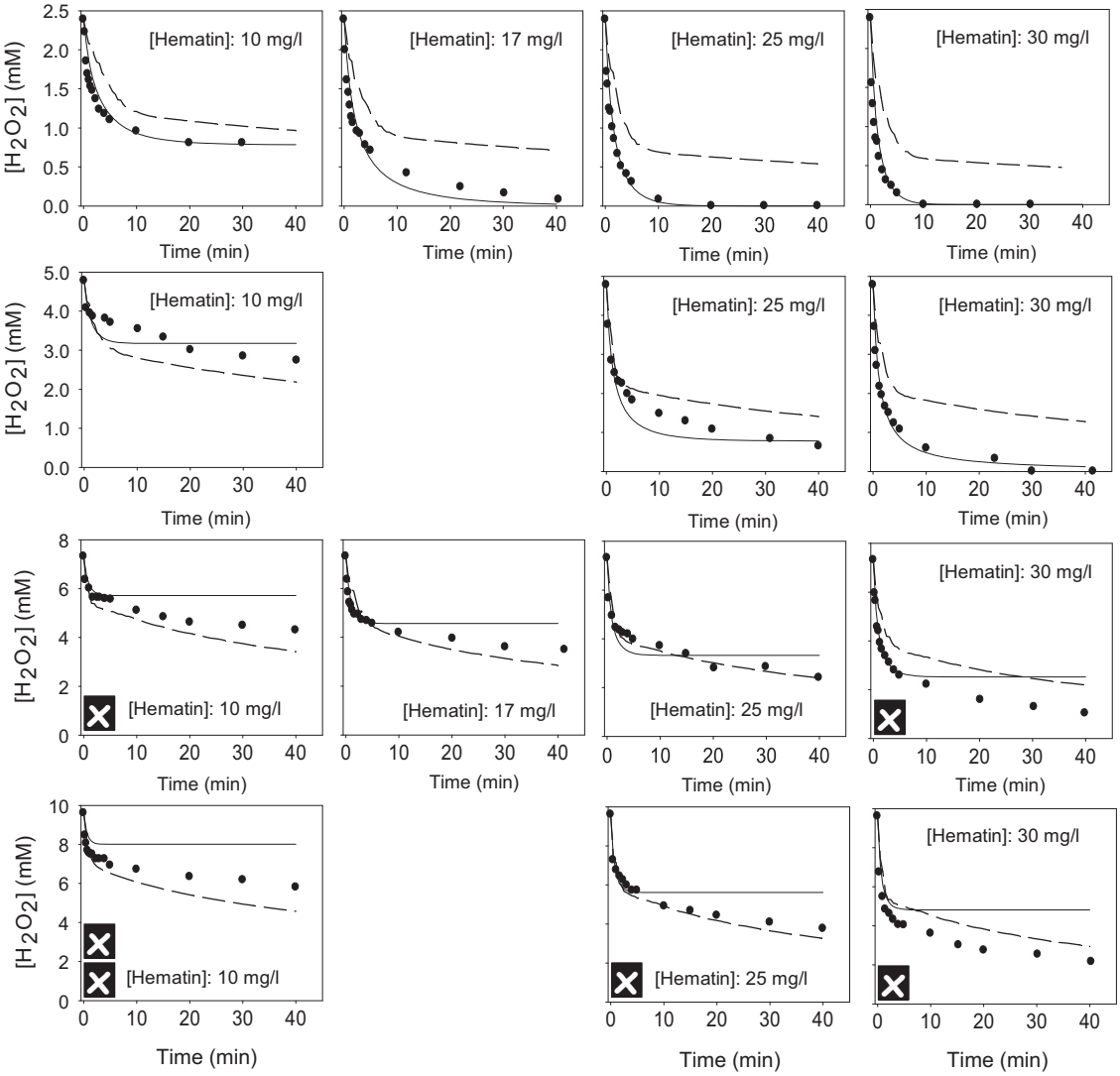

Fig. 3. Experimental (points) and modelled (lines) concentration profiles of hematin-mediated H_2O_2 dismutation. Continues lines: C-model. Dash lines: PC-model. Graphs marked with one or double cross represents model extrapolations, whose data had to be excluded for parametrization task of catalatic or both models, respectively.

$$\underbrace{\text{aa Por Fe(III)}}_{E_0} + OO^{\cdot -} \leftrightarrow \underbrace{[\text{aa Por Fe(III)} - OO^{\cdot -}]}_{E_3}$$

$$\underbrace{[\text{aa Por Fe(III)} - OO^{\cdot -}]}_{E_3} \leftrightarrow [\text{aa Por Fe(II)} - O_2]$$

$$[\text{aa Por Fe(II)} - O_2] \leftrightarrow \underbrace{\text{aa Por Fe(II)} + O_2}_{E_{Fe}}$$

Ferrous porphyrin can be oxidized by H_2O_2 into Por(IV)-OH i.e. E_2 thus returning into the main cycle (Vlasits et al., 2010). The rate of decay of Compound III (E_3) of heme peroxidases either to the resting state or to E_2 limits its recovery into the main cycle (Vlasits et al., 2010). Both reactions were considered as hematin reversible inactivation mechanisms targeted by superoxide generated in the pseudo-catalatic model (dash lines in Scheme 1).

Table 1 shows the values of rate constants obtained after parametrization and Fig. 3 presents simulated $[H_2O_2]$ profiles (dashed lines). The biphasic behaviour of profiles at high peroxide concentrations is predicted adequately using this model. The pseudo-catalatic model seems to be valid for a higher range of conditions compared to the catalatic model. Optimized k_1 was four orders of magnitude lower than k_1 reported for peroxidases (an expected result). Despite k_{2b} and k_5 values could not be optimized, both tended to values higher than k_1 indicating greater affinity of E_1 and E_2 intermediates to peroxide compared to monofunctional peroxidases.

Simulation of profiles by the pseudo-catalatic model indicated that hematin concentration does not affect peroxide consumption rates. This is evident for profiles at high hematin concentrations when experimental peroxide consumptions are higher than simulated ones. The root of differences may include the generation of inorganic radicals such as $OH^{\cdot}$ or $OOH^{\cdot}$. In a prior UV–Visible study of hematin-H_2O_2, the formation of inactive μ-oxo dimer has been discarded (Córdoba et al., 2012b). Nevertheless, hematin can form reversible aggregates by hydrogen bonds or ester formation between a carboxylate group and the —OH of the fifth coordination position. Fig. 4 shows potential structures of dimers, trimers and tetramers of hematin. Ester formation between hematin molecules can take place at the alkaline condition in the absence of H_2O_2. When H_2O_2 is added to the system, the species hem–Fe–OOH may emerge after dissociation of the ester bond. This species can generate hydroxyl radicals $OH^{\cdot}$ and anions as OH^- or OOH^- during

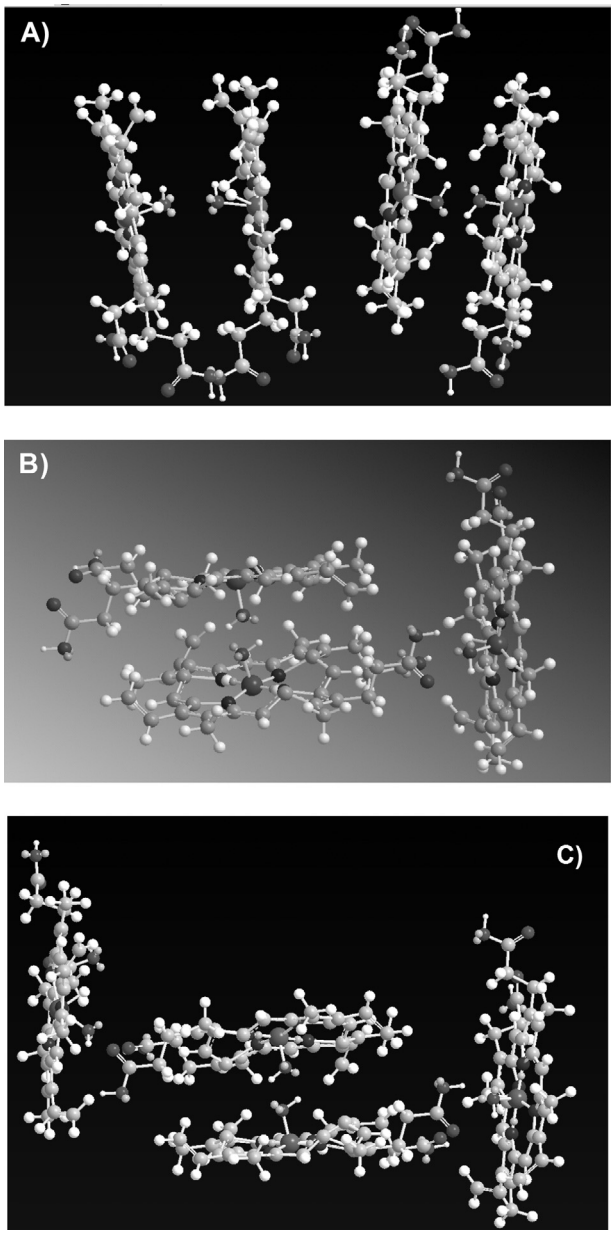

Fig. 4. (A) Hematin dimers due to hydrogen bonds interactions involving carboxylic groups (left) and hydroxyl groups (right). (B) Hematin trimers and (C) Hematin tetramers.

its decomposition, all of them triggering additional H_2O_2 dismutation (Paolo Zucca and Sanjust, 2014). At high hematin concentration the postulated H_2O_2-mediated aggregates decomposition may explain the discrepancy of the pseudo-catalatic model with experimental profiles.

Potential hematin bleaching may be accompanied by releasing of Fe^{3+}, which can promote H_2O_2 consumption by a Fenton-like mechanism (Magario et al., 2012) thus accounting for model deviations observed at high peroxide concentrations.

4.3. Kinetics of OII decolourization

Initial rates of OII removal were consistent with a reversible inactivation by non-productive interaction between hematin and OII (Pirillo et al., 2010b). These inactivation routes were checked in P-C and P-PC models. The P-C model gave a good fit (chi-square lower than weighted residuals). However, the kinetics constants were statistically insignificant in all estimation procedures (results no shown). Thus, in order to improve these results an alternative but irreversible OII-inactivation route due to an unproductive coordination to E_1 was tested (k_{ii}) (Pirillo et al., 2010a). Table 2 presents initial guesses and optimized rate constants values for P-C and P-PC model. A good fit have been obtained with both models. Decolourization and inactivation rate constants (k_2, k_3 and k_{ii} or k_i and k_{-i}) could be parametrized with significance. Nevertheless, the peroxidatic-pseudocatalatic (P-PC) model gave higher statistical support. Optimized rate constants in the P-PC model decreased about 25% regarding initial guesses thus maintaining the initial ratios between them (k_2/k_3 and k_i/k_{-i}).

Decolourization modelled vs. experimental data are shown in Figs. 5 and 6. Peroxidatic-pseudo-catalatic model predictions were closer to experimental findings. This model was selected as the most suitable to predict the kinetic behaviour of decolourization using hematin.

Thus, OII mediated inactivation could properly describe decolourization until about 50% OII conversion. Nevertheless, model deviations appeared at this point indicating the involvement of products in kinetics.

In almost every run experimental decolourization was always higher than predicted after 50% OII conversion. Some goodness of fit improvement was observed at e.g. [OII]:200 mg/l; [H_2O_2]:7.31 mM, 9.6 mM. Now, these behaviour can be attributed to: (1) the attack of $OO^{\cdot-}$ to OII causing cooperative decolourization (Munter, 2001); or (2) an overvalue of k_{Fe} and k_6, i.e. phenolics inhibit alternative routes of H_2O_2 consumption in line with HRP behaviour (Hernández-Ruiz et al., 2001; Hiner et al., 2001;

Table 2
Initial guesses and optimized rate constants values.

P-C Model (peroxidatic-catalatic)			P-PC Model (peroxidatic-pseudocatalatic)		
	Initial guess (mM^{-1} min^{-1})	Optimized		Initial guess (mM^{-1} min^{-1})	Optimized
k_1	16.4*	16.4	k_1	16.4*	16.4
k_2	20.9	$449_{\pm 100}$	k_2	7694	$1712_{\pm 162}$
k_3	2.09	$52_{\pm 11}$	k_3	769.4	$207_{\pm 43}$
k_i	0*	–	k_i	16.4	$4.7_{\pm 0.7}$
k_{-i}	0*	–	k_{-i}	6.9	$1.15_{\pm 0.28}$
k_{ii}	0.01	$8.3_{\pm 0.8}$	k_{ii}	0*	–
k_4	20.9*	20.9	k_{2b}	60.2*	60.2
k_{Bl}	0.33*	0.33	k_5	90.3*	90.3
			k_{Fe}	3.49*	3.49
			k_6	0.026*	0.026
Initial guess of σ^2		0.1^2		0.1^2	
Optimized σ^2		$0.135^2_{\pm 0.012}$		$0.087^2_{\pm 0.004}$	
Residuals		146.5		399.1	
χ^2 (95%)		342.5		441.3	

* Fixed value during parameter estimation.

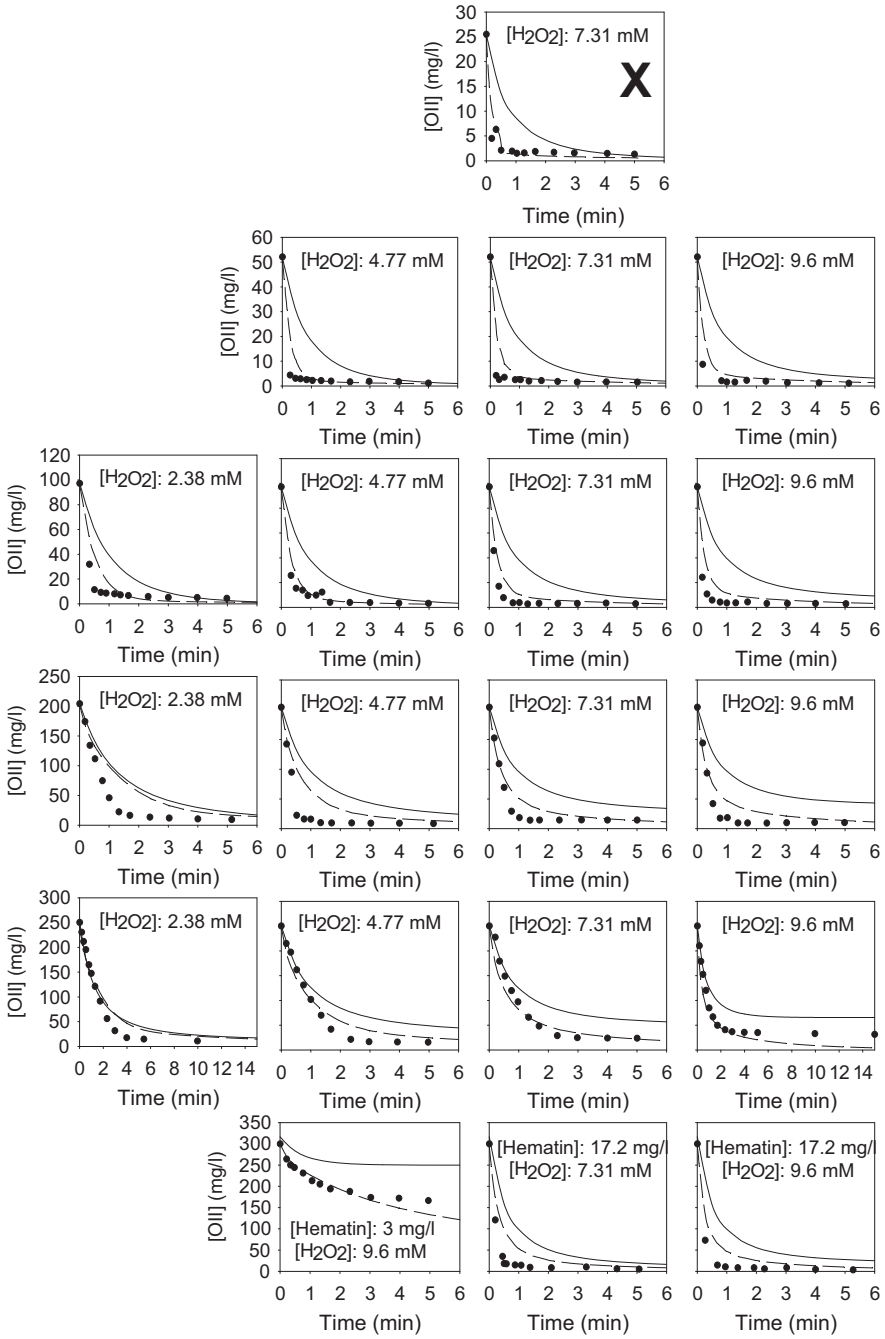

Fig. 5. Experimental (points) and modelled (lines) concentration profiles of hematin-mediated OII decolourization. Continues lines: P-C model. Dash lines: P-PC model. In plots without hematin concentration specified, [Hematin]: 10 mg/l. Graphs marked with one cross represents model extrapolations, whose data had to be excluded for parametrization task of catalatic-peroxidatic model.

Vlasits et al., 2010). It seems that evidence favours route 2. Nevertheless, previous molecular modelling studies have confirmed that E_1 can interact either with H_2O_2 or antraquinonic dyes.

At high OII and H_2O_2 concentrations modelled data showed important deviation – e.g. [OII]:400 mg/l; [H_2O_2]:7.31 mM, 9.6 mM-. Previous UV–Visible and FTIR studies of OII oxidation products have confirmed the formation of OII-degraded structures capable to be oxidized by H_2O_2/Hematin system (Fig. 7) (Córdoba et al., 2012a). Therefore, this overestimation may be caused by hematin catalysed oxidation of OII-degraded products rather than the OII structure, thus becoming important only when OII and H_2O_2 concentrations are both high.

According to the peroxidatic cycle, one H_2O_2 molecule is needed for the degradation of two OII molecules. Fig. 8 presents experimental vs. modelled conversion of H_2O_2 after 40 min decolourization time (the corresponding OII profiles during reaction are presented in Figs. 5 and 6). Simulated conversions showed a pattern, which was practically unaffected by the applied OII concentration and even very similar to the one obtained without OII. According to the P-PC model, most H_2O_2 consumption was due to the pseudo-catalatic pathway since H_2O_2 was always applied in excess. Now, the differences found with experimental conversion give additional information. At high H_2O_2 concentrations (>4.8 mM) experimental conversions were always lower than

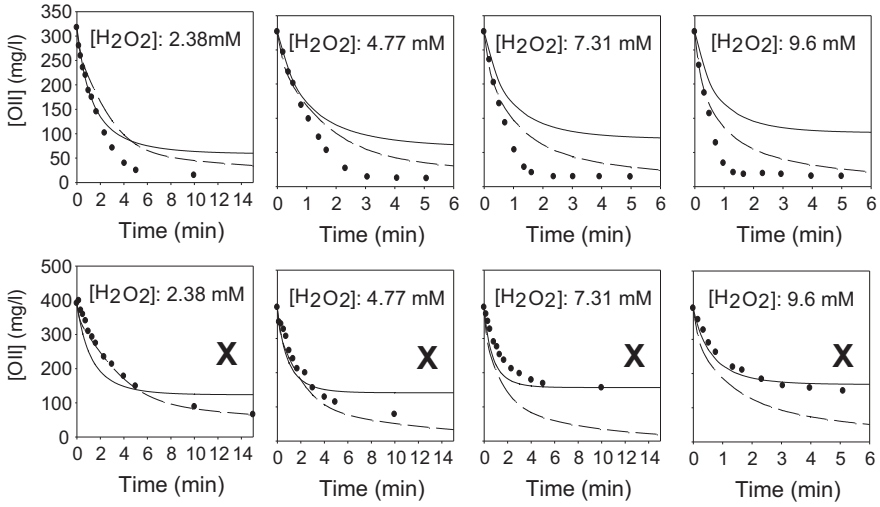

Fig. 6. Experimental (points) and modelled (lines) concentration profiles of hematin-mediated OII decolourization. Continues lines: P-C model. Dash lines: P-PC model. [Hematin]: 10 mg/l. Graphs marked with one cross represents model extrapolations, whose data had to be excluded for parametrization task of peroxidatic-catalatic model.

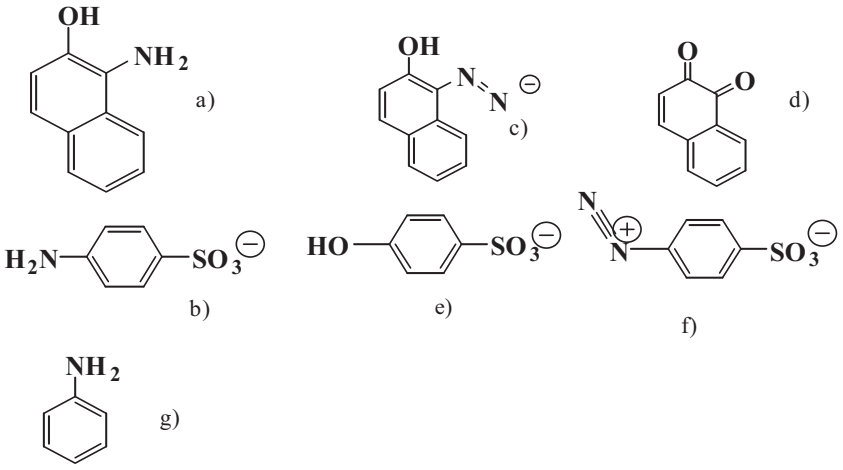

Fig. 7. OII-degradated products capable to be ozidized by H_2O_2/Hematin system by hydrogen abstraction. (a) 1−amino 2−naphtol; (b) sulfanilate; (c) 1−diazo 2−naphtol; (d) 1,2−naphtoquinone; (e) 4−hydroxi bencenesulfonate; (f) 4−diazo bencenesulfonate; (g) aniline.

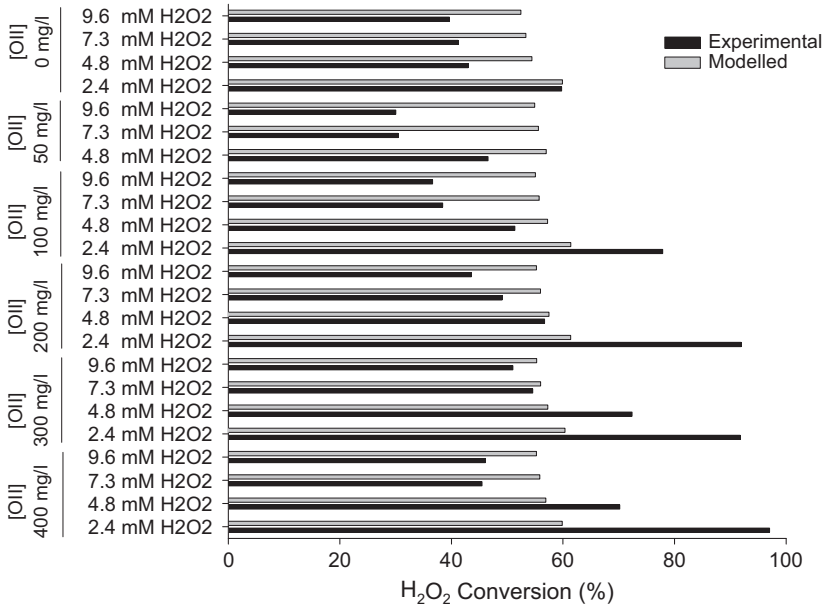

Fig. 8. Experimental and modelled H_2O_2 consumption after hematin-mediated OII decolourization.

simulated. Probably, extra hematin deactivation by e.g. bleaching - superoxide attack to the pyrrole ring of hematin- is being missed in the model. On the other hand, at low H_2O_2 concentration (<4.8 mM) and OII concentration (>0.28 mM), experimental conversions were higher than predicted and clearly increasing with the increase of the applied OII concentration. This observation gives support to the hematin-catalysed oxidation of OII-degraded products as discussed above. Evidently, a more complex mechanism is required to model the overall range of experimental conditions. More secondary reactions should be taken into account. This kind of studies would be the center of forthcoming studies.

5. Conclusions

In order to describe the kinetic behaviour of the hematin-catalysed decolourization of Orange II solutions, two different kinetic models were proposed and validated. The inspection of initial rates not only gave support to the proposed mechanisms (thus enabling reliable estimates of most significant rate constants) but also allowed to elucidate hematin inhibition by non-productive coordination of the OII's molecules.

Hematin catalysed H_2O_2 dismutation to dioxygen was detected as an important and inefficient parallel route. The most straightforward catalatic model was unable to describe the biphasic nature of H_2O_2 decomposition experimental profiles. Therefore, a more complicated pathway involving the generation of superoxide and subsequent coordination to hematin ferryl species into ferrous hematin was proposed. This pathway could explain the above mentioned behaviour. A H_2O_2-mediated breakdown of hematin aggregates formed under alkaline conditions was postulated in order to explain the underestimation of the model at high hematin to H_2O_2 ratios.

The peroxidatic-pseudo catalatic model was the most suitable to describe the observed decolourization kinetics at a wide range of conditions (25–400 mg/l OII concentration, 2.4–10 mM H_2O_2 concentration and 3–17 mg/l hematin concentration) at room temperature and alkaline pH (10.6). While this model was based on the peroxidatic action, it included two reversible inactivation routes due to H_2O_2 and Orange II – E_{Fe} formation and E-OII formation-. Rate constant of OII-involved reactions were optimized with high statistical significance. Model deviations were discussed taking into consideration the direct involvement of superoxide in OII degradation as well as in hematin bleaching. At high OII concentrations the model underestimated hydrogen peroxide but overestimated OII consumptions. Reaction products of Orange II degradation may be better substrates for hematin than the OII molecules for further hematin-mediated oxidation.

The consideration of OII oxidation products and their further oxidation in decolourization kinetics are required to improve simulations. Moreover, hematin immobilization onto a solid support can be tested in order to overcome unproductive OII coordination.

Acknowledgment

The authors acknowledge the financial support of the National Council of Scientific and Technical Research (CONICET), the National Agency of Scientific and Technological Promotion (ANPCyT-PICT2010-0788 PRH-UNC-3), and the National University of Córdoba (Argentina). Furthermore, the authors acknowledge: the collaboration of PhD Mariano Asteasuain and PhD Adriana Brandolín (Planta Piloto de Ingeniería Química, PLAPIQUI-CONICET, Bahía Blanca, Argentina) in all activities involving gPROMS calculations; and the kind contribution of the Industrial Chemistry Department of the Faculty of Exact, Physical and Natural Sciences of the National University of Córdoba for providing lab installations.

References

Akkara, J.A., Wang, J., Yang, D.P., Gonsalves, K.E., 2000. Hematin-catalyzed polymerization of phenol compounds. Macromolecules 33, 2377–2382.
Ambrosio, K., Rueda, E., Ferreira, M.L., 2004. Magnetite-supported hematin as a biomimetic of horseradish peroxidase in phenol removal by polymerization. Biocatal. Biotrans. 22, 35–44.
Babuponnusami, A., Muthukumar, K., 2014. A review on Fenton and improvements to the Fenton process for wastewater treatment. J. Environ. Chem. Eng. 2, 557–572.
Bell, S.E.J., Cooke, P.R., Inchley, P., Leanord, D.R., Lindsay Smith, J.R., Robbins, A., 1991. Oxoiron(IV) porphyrins derived from charged iron(III) tetraarylporphyrins and chemical oxidants in aqueous and methanolic solutions. J. Chem. Soc. Perkin Trans. 2, 549–559.
Bhunia, A., Durani, S., Wangikar, P.P., 2001. Horseradish peroxidase catalyzed degradation of industrially important dyes. Biotechnol. Bioeng. 72, 562–567.
Bruice, T.C., Balasubramanian, P.N., Lee, R.W., Smith, J.R.L., 1988. The mechanism of hydroperoxide O—O bond scission on reaction of hydroperoxides with iron(III) porphyrins. J. Am. Chem. Soc. 110, 7890–7892.
Buchanan, I.D., Nicell, J.A., 1997. Model development for horseradish peroxidase catalyzed removal of aqueous phenol. Biotechnol. Bioeng. 54, 251–261.
Cardona, M., Osorio, J., Quintero, J., 2009. Degradation of industrial dyes with white rot fungi. Degrad. Color. Ind. con hongos ligninolíticos, 27–37.
Centro Panamericano de Ingeniería Sanitaria y Ciencias del Ambiente, 1994. Informe técnico sobre la minimización de residuos textiles.
Centro Panamericano de Ingeniería Sanitaria y Ciencias del Ambiente, 1997. Informe técnico sobre minimización de residuos en la industria textil.
Chen, J.X., Zhu, L., 2010. Degradation mechanism of Orange II in UV-Fenton process with hydroxyl-Fe-pillared bentonite as heterogeneous catalyst. In: 2010 International Conference on Advances in Energy Engineering, ICAEE 2010, pp. 281–284.
Córdoba, A., Magario, I., Ferreira, M.L., 2012a. Evaluation of hematin-catalyzed Orange II degradation as a potential alternative to horseradish peroxidase. Int. Biodeterior. Biodegrad. 73, 60–72.
Córdoba, A., Magario, I., Ferreira, M.L., 2012b. Experimental design and MM2-PM6 molecular modelling of hematin as a peroxidase-like catalyst in Alizarin Red S degradation. J. Mol. Catal. A Chem. 355, 44–60.
Córdoba, A., Alasino, N., Asteasuain, M., Magario, I., Ferreira, M.L., 2015. Mechanistic evaluation of hematin action as a horseradish peroxidase biomimetic on the 4-aminoantipyrine/phenol oxidation reaction. Chem. Eng. Sci. 129, 249–259.
Cunningham, I.D., Danks, T.N., Hay, J.N., Hamerton, I., Gunathilagan, S., 2001. Evidence for parallel destructive, and competitive epoxidation and dismutation pathways in metalloporphyrin-catalysed alkene oxidation by hydrogen peroxide. Tetrahedron 57, 6847–6853.
Daneshvar, N., Rabbani, M., Modirshahla, N., Behnajady, M.A., 2004. Kinetic modeling of photocatalytic degradation of Acid Red 27 in UV/TiO_2 process. J. Photochem. Photobiol. A Chem. 168, 39–45.
Daneshvar, N., Aber, S., Hosseinzadeh, F., 2008. Study of C.I. Acid Orange 7 removal in contaminated water by photo oxidation processes. Glob. Nest J. 10, 16–23.
Dunford, H.B., 1999. Heme Peroxidases. John Wiley, VCH, USA.
Dunford, H.B., 2002. Oxidations of iron(II)/(III) by hydrogen peroxide: From aquo to enzyme. Coord. Chem. Rev. 233–234, 311–318.
Gómez, J.L., Bódalo, A., Gómez, E., Bastida, J., Hidalgo, A.M., Gómez, M., 2006. Immobilization of peroxidases on glass beads: an improved alternative for phenol removal. Enzyme Microb. Technol. 39, 1016–1022.
Gong, Y.H., Zhang, H., Li, Y.L., Xiang, L.J., Royer, S., Valange, S., Barrault, J., 2010. Evaluation of heterogeneous photo-Fenton oxidation of Orange II using response surface methodology. Water Sci. Technol. 62, 1320–1326.
Hai, F.I., Yamamoto, K., Nakajima, F., Fukushi, K., 2009. Factors governing performance of continuous fungal reactor during non-sterile operation – the case of a membrane bioreactor treating textile wastewater. Chemosphere 74, 810–817.
Hamid, M., Khalilur, R., 2009. Potential applications of peroxidases. Food Chem. 115, 1177–1186.
Hammami, S., Bellakhal, N., Oturan, N., Oturan, M.A., Dachraoui, M., 2008. Degradation of Acid Orange 7 by electrochemically generated ·OH radicals in acidic aqueous medium using a boron-doped diamond or platinum anode: a mechanistic study. Chemosphere 73, 678–684.
Hernández-Ruiz, J., Arnao, M.B., Hiner, A.N.P., García-Cánovas, F., Acosta, M., 2001. Catalase-like activity of horseradish peroxidase: relationship to enzyme inactivation by H_2O_2. Biochem. J. 354, 107–114.
Hiner, A.N.P., Hernández-Ruiz, J., Williams, G.A., Arnao, M.B., García-Cánovas, F., Acosta, M., 2001. Catalase-like oxygen production by horseradish peroxidase must predominantly be an enzyme-catalyzed reaction. Arch. Biochem. Biophys. 392, 295–302.
Hodges, G., Lindsay Smith, J.R., Oakes, J., 1997. Metalloporphyrin-catalysed oxidation of azonaphthol dyes: The mechanism of oxidative bleaching by oxoiron(IV) porphyrins in aqueous solution. Stud. Surf. Sci. Catal. 110, 653–662.
Hunger, K., 2003. Industrial Dyes: Chemistry, Properties, Applications. Weinheim.
Lachheb, H., Puzenat, E., Houas, A., Ksibi, M., Elaloui, E., Guillard, C., Herrmann, J.M., 2002. Photocatalytic degradation of various types of dyes (Alizarin S, Crocein

Orange G, Methyl Red, Congo Red, Methylene Blue) in water by UV-irradiated titania. Appl. Catal. B 39, 75–90.
Liang, X., Zhong, Y., Zhu, S., Zhu, J., Yuan, P., He, H., Zhang, J., 2010. The decolorization of Acid Orange II in non-homogeneous Fenton reaction catalyzed by natural vanadium-titanium magnetite. J. Hazard. Mater. 181, 112–120.
Lodha, B., Chaudhari, S., 2007. Optimization of Fenton-biological treatment scheme for the treatment of aqueous dye solutions. J. Hazard. Mater. 148, 459–466.
Loew, G.H., Harris, D.L., Dupuis, M., 1997. Calculations of the structure and spectra of the putative transient peroxide intermediates of peroxidases. J. Mol. Struct. THEOCHEM 398–399, 497–505.
López, C., Moreira, M.T., Feijoo, G., Lema, J.M., 2004a. Dye decolorization by manganese peroxidase in an enzymatic membrane bioreactor. Biotechnol. Prog. 20, 74–81.
López, C., Valade, A.G., Combourieu, B., Mielgo, I., Bouchon, B., Lema, J.M., 2004b. Mechanism of enzymatic degradation of the azo dye Orange II determined by ex situ 1H nuclear magnetic resonance and electrospray ionization-ion trap mass spectrometry. Anal. Biochem. 335, 135–149.
MacKay, A.A., Pignatello, J.J., 2001. Application of Fenton-based reactions for treating dye wastewaters: Stability of sulfonated azo dyes in the presence of iron(III). Helv. Chim. Acta 84, 2589–2600.
Magario, I., García Einschlag, F.S., Rueda, E.H., Zygadlo, J., Ferreira, M.L., 2012. Mechanisms of radical generation in the removal of phenol derivatives and pigments using different Fe-based catalytic systems. J. Mol. Catal. A Chem. 352, 1–20.
Modirshahla, N., Behnajady, M.A., 2006. Photooxidative degradation of Malachite Green (MG) by UV/H_2O_2: influence of operational parameters and kinetic modeling. Dye. Pigment. 70, 54–59.
Munter, R., 2001. Advances oxidation processes – current status and prospects. Proc. Est. Acad. Sci. Chem. 50, 59–80.
Nam, W., Han, H.J., Oh, S.Y., Lee, Y.J., Choi, M.H., Han, S.Y., Kim, C., Woo, S.K., Shin, W., 2000. New insights into the mechanisms of O—O bond cleavage of hydrogen peroxide and tert-alkyl hydroperoxides by iron(III) porphyrin complexes. J. Am. Chem. Soc. 122, 8677–8684.
Nam, S., Renganathan, V., Tratnyek, P.G., 2001. Substituent effects on azo dye oxidation by the FeIII-EDTA-H_2O_2 system. Chemosphere 45, 59–65.
Nicell, J.A., 1994. Kinetics of horseradish peroxidase-catalysed polymerization and precipitation of aqueous 4-chlorophenol. J. Chem. Technol. Biotechnol. 60, 203–215.
Nicell, J.A., Wright, H., 1997. A model of peroxidase activity with inhibition by hydrogen peroxide. Enzyme Microb. Technol. 21, 302–310.
Nicell, J.A., Saadi, K.W., Buchanan, I.D., 1995. Phenol polymerization and precipitation by horseradish peroxidase enzyme and an additive. Bioresour. Technol. 54, 5–16.
Oh-Kyu Lee, 2002. Mechanistic Studies of the Oxidation of Lignin and Cellulose Models. (2003). Electronic theses and Dissertations.
Paolo Zucca, P., Sanjust, E., 2014. Inorganic materials as supports for covalent enzyme immobilization: methods and mechanisms. Molecules 19, 14139–14194.
Pirillo, S., Einschlag, F.S.G., Ferreira, M.L., Rueda, E.H., 2010a. Eriochrome Blue Black R and Fluorescein degradation by hydrogen peroxide oxidation with horseradish peroxidase and hematin as biocatalysts. J. Mol. Catal. B Enzym. 66, 63–71.
Pirillo, S., García Einschlag, F.S., Rueda, E.H., Ferreira, M.L., 2010b. Horseradish peroxidase and hematin as biocatalysts for alizarin degradation using hydrogen peroxide. Ind. Eng. Chem. Res. 49, 6745–6752.
Process Systems Enterprise, 2004. Advanced User Guide Gproms. Process Systems Enterprise.
Rafiquzzaman, M., Komagoe, K., Tamagake, K., 1995. Comparative catalytic activity of hemin and hematin in the breakdown of methyllinoleate hydroperoxide and peroxidation of methyllinoleate in methanol. Chem. Pharm. Bull. 43, 905–909.
Rebelo, S., Pereira, M., Simoes, M., Neves, M., Cavaleiro, J., 2005. Mechanistic studies on metalloporphyrin epoxidation reactions with hydrogen peroxide: evidence for two active oxidative species. J. Catal. 234, 76–87.
Reihmann, M., Ritter, H., 2006. Synthesis of phenol polymers using peroxidases. Adv. Polym. Sci. 194, 1–49.
Rich, P.R., Iwaki, M., 2007. A comparison of catalytic site intermediates of cytochrome c oxidase and peroxidases. Biochemistry 72, 1047–1055.
Saratale, R.G., Saratale, G.D., Chang, J.S., Govindwar, S.P., 2011. Bacterial decolorization and degradation of azo dyes: A review. J. Taiwan Inst. Chem. Eng. 42, 138–157.
Sheldon, Roger A. (Ed.), 1994. Metalloporphyrins in Catalytic Oxidations. ISBN:0-8247-9228-9.
Sleiman, M., Vildozo, D., Ferronato, C., Chovelon, J.-M., 2007. Photocatalytic degradation of azo dye Metanil Yellow: optimization and kinetic modeling using a chemometric approach. Appl. Catal. B Environ. 77, 1–11.
Song, C., Zhang, J., 2008. Electrocatalytic oxygen reduction reaction. In: PEM Fuel Cell Electrocatalysts and Catalyst Layers. Springer, London, London, pp. 89–134.
Stephenson, A.T., Bell, N.A., 2005. A study of the mechanism and kinetics ofcyclooctene epoxidation catalyzed by iron(III) tetrakispentafluorophenylporphyrin. J. Am. Chem. Soc. 127, 8635–8643.
Stephenson, N.A., Bell, A.T., 2007a. Mechanistic study of iron(III) tetrakis (pentafluorophenyl)porphyrin triflate (F20TPP)Fe(OTf) catalyzed cyclooctene epoxidation by hydrogen peroxide. Inorg. Chem. 46, 2278–2285.
Stephenson, N.A., Bell, A.T., 2007b. Mechanistic insights into iron porphyrin-catalyzed olefin epoxidation by hydrogen peroxide: factors controlling activity and selectivity. J. Mol. Catal. A Chem. 275, 54–62.
Tizaoui, C., Grima, N., 2011. Kinetics of the ozone oxidation of Reactive Orange 16 azo-dye in aqueous solution. Chem. Eng. J. 173, 463–473.
Traylor, T.G., Xu, F., 1987. A biomimetic model for catalase: the mechanisms of reaction of hydrogen peroxide and hydroperoxides with iron(III) porphyrins. J. Am. Chem. Soc. 109, 6201–6202.
Traylor, T.G., Xu, F., 1990. Mechanisms of reactions of iron(III) porphyrins with hydrogen peroxide and hydroperoxides: solvent and solvent isotope effects. J. Am. Chem. Soc. 112, 178–186.
Ulson de Souza, S.M.A.G., Forgiarini, E., Ulson de Souza, A.A., 2007. Toxicity of textile dyes and their degradation by the enzyme horseradish peroxidase (HRP). J. Hazard. Mater. 147, 1073–1078.
Van Der Zee, J., Barr, D.P., Mason, R.P., 1996. ESR spin trapping investigation of radical formation from the reaction between hematin and tert-butyl hydroperoxide. Free Radic. Biol. Med. 20, 199–206. http://dx.doi.org/10.1016/0891-5849(95)02031-4.
Veitch, N.C., 2004. Horseradish peroxidase: a modern view of a classic enzyme. Phytochemistry 65, 249–259.
Vlasits, J., Jakopitsch, C., Bernroitner, M., Zamocky, M., Furtmüller, P.G., Obinger, C., 2010. Mechanisms of catalase activity of heme peroxidases. Arch. Biochem. Biophys. 500, 74–81.
Vojinovic, V., Azevedo, A.M., Martins, V.C.B., Cabral, J.M.S., Gibson, T.D., Fonseca, L.P., 2004. Assay of H_2O_2 by HRP catalysed co-oxidation of phenol-4-sulphonic acid and 4-aminoantipyrine: characterisation and optimisation. J. Mol. Catal. B Enzym. 28, 129–135.
Wagner, M., Nicell, J.A., 2002. Detoxification of phenolic solutions with horseradish peroxidase and hydrogen peroxide. Water Res. 36, 4041–4052.
Yousefi, V., Kariminia, H.R., 2010. Statistical analysis for enzymatic decolorization of acid orange 7 by Coprinus cinereus peroxidase. Int. Biodeterior. Biodegrad. 64, 245–252.
Zucca, P., Vinci, C., Sollai, F., Rescigno, A., Sanjust, E., 2008. Degradation of Alizarin Red S under mild experimental conditions by immobilized 5,10,15,20-tetrakis (4-sulfonatophenyl)porphine-Mn(III) as a biomimetic peroxidase-like catalyst. J. Mol. Catal. A Chem. 288, 97–102.